# scientific reports



# **OPEN**

# Morphologic and functional alterations in the parasagittal dural space in mild cognitive impairment

Bio Joo¹, Mina Park<sup>1⊠</sup>, Song Soo Kim¹, Sung Jun Ahn¹, Han-Kyeol Kim², Hanna Cho², Chul Hyoung Lyoo² & Sang Hyun Suh¹

This study aimed to identify morphologic and functional differences in the parasagittal dural space (PSD) between patients with mild cognitive impairment (MCI) and cognitively unimpaired participants using dynamic contrast-enhanced MRI (DCE MRI). A total of 29 MCI patients and nine controls underwent structural MRI and DCE MRI, where PSD volume and parameters such as peak wash-in rate and time to first peak enhancement were assessed. MCI patients had significantly larger PSD volume (P = 0.023), a lower peak wash-in rate (P < 0.001), and delayed time to first peak (P = 0.001) compared to controls. In multivariate regression analysis, PSD volume ( $\beta$  = -0.579, 95% CI [-1.072 – -0.086], P = 0.023) and wash-out rate ( $\beta = -3.293$ , 95% CI [-6.351 - -0.235], P = 0.036) were significantly associated with the Mini-Mental State Examination (MMSE) score. Additionally, a lower peak wash-in rate correlated significantly with lower cognitive performance, as measured by the Montreal Cognitive Assessment (MoCA) (P = 0.043). This association highlights a potential link between meningeal lymphatic dysfunction and cognitive decline, suggesting that PSD alterations could reflect early stages of neurodegenerative changes. In conclusion, these PSD structural and functional alterations in MCI patients may serve as early imaging markers, helping in the assessment of disease severity in neurodegenerative conditions such as Alzheimer's disease. This insight into meningeal lymphatic dysfunction provides a promising direction for early diagnosis and monitoring of cognitive impairment.

**Keywords** Mild cognitive impairment, Dementia, Meningeal lymphatic system, Magnetic resonance imaging, Dynamic contrast-enhanced imaging

# Abbreviations

MCI mild cognitive impairment PSD parasagittal dural space

DCE MRI dynamic contrast-enhanced magnetic resonance imaging

MoCA montreal cognitive assessment MRI magnetic resonance imaging

ICV intracranial volume

MMSE mini-mental state examination

Since the recent discovery of true lymphatic vessels in the dura mater, situated mainly along the dural venous sinuses, interest in the meningeal lymphatic system among researchers has significantly increased<sup>1,2</sup>. It has been reported to play a crucial role in the drainage of interstitial fluid (ISF), cerebrospinal fluid (CSF), and metabolic wastes from the central nervous system (CNS) to the extracranial system, as well as the peripheral surveillance of CNS antigens<sup>3,4</sup>. Dysfunction in the meningeal lymphatic system may result in the accumulation of metabolites and misfolded proteins in the CNS system. This can disrupt CNS homeostasis and ultimately lead to the development of neurodegenerative diseases including Alzheimer's and Parkinson's disease<sup>5–8</sup>. Thus, assessing the meningeal lymphatic system in vivo is of considerable importance.

The parasagittal dural space (PSD), located around the superior sagittal sinus and characterized by irregular, loose tissue rich in collagen and fibronectin, is understood to house this meningeal lymphatic system, along with arachnoid granulations<sup>7,9–11</sup>. Some previous studies have explored the use of brain magnetic resonance imaging (MRI) with intrathecal injection of a gadolinium contrast agent to investigate the meningeal lymphatic

<sup>1</sup>Department of Radiology, Gangnam Severance Hospital, Yonsei University College of Medicine, Seoul, Republic of Korea. <sup>2</sup>Department of Neurology, Gangnam Severance Hospital, Yonsei University College of Medicine, Seoul, Republic of Korea. <sup>⊠</sup>email: to.minapark@yuhs.ac

vessels in the PSD of humans<sup>9,12</sup>. The invasive nature of this method has, nevertheless, limited its application in clinical practice. Therefore, various imaging techniques have been experimented as a non-invasive or less invasive method. These include both volumetric approaches, including contrast-enhanced T1-weighted black blood imaging, T2-weighted imaging, and fluid attenuated inversion recovery (FLAIR) imaging<sup>13–16</sup>, and functional approaches using dynamic contrast-enhanced (DCE) MRI with intravenous administration of a contrast agent<sup>17–19</sup>. In a previous study using DCE MRI, the wash-out rate specifically has been reported to represent the meningeal lymphatic function, showing delayed drainage of the PSD within the aged population compared to their younger counterparts<sup>19</sup>. However, none of the imaging studies on meningeal lymphatics have been specifically applied to the evaluation of mild cognitive impairment (MCI), an early clinical stage in the Alzheimer's disease spectrum.

In this study, we hypothesized that (1) in patients with MCI, contrast agent dynamics in the PSD would be impaired, manifesting as a delayed contrast influx on DCE MRI, leading to PSD enlargement; and (2) these morphologic and functional changes in the PSD would be associated with the severity of cognitive impairment. Thus, we aimed to assess morphologic and functional differences between MCI patients and cognitively unimpaired participants by measuring PSD volume on structural MRI and evaluating various DCE MRI-derived parameters. Additionally, we investigated whether PSD volume and contrast agent dynamics independently correlate with the severity of cognitive impairment, after adjusting for other clinical and morphologic factors.

# Materials and methods

This prospective study was approved by the Gangnam Severance Hospital Institutional Review Board (IRB No. 3-2020-0162) and was conducted following the Declaration of Helsinki. Informed consent was obtained from all participants.

# Study participants

This study enrolled a total of ten cognitively unimpaired elderly participants and 30 patients with MCI between Oct 2020 and March 2022. Inclusion criteria of cognitively unimpaired elderly participants were as follows: (i) with no history of neurological or psychiatric disease; (ii) with intact activities of daily living; (iii) with minimental state examination (MMSE) scores of  $\geq$ 26; and (iv) an estimated glomerular filtration rate of  $\geq$ 60 ml/min/1.73m² tested within a year. Inclusion criteria for MCI patients in our study were as follows: (i) a clinical diagnosis of MCI made by a neurologist based on the Petersen criteria, which includes (1) subjective cognitive decline, (2) the Montreal Cognitive Assessment (MoCA) score of  $\leq$ 25, and (3) no significant impairment in daily activities; and (ii) an estimated glomerular filtration rate of  $\geq$ 60 ml/min/1.73 m², tested within a year<sup>20,21</sup>. Exclusion criteria for both cognitively unimpaired elderly participants and MCI patients were as follows: (i) significantly abnormal findings or severe artifact on brain MRI; and (ii) a physician-indicated contraindication to an MRI examination. Of them, one cognitively unimpaired elderly participant and one MCI patient were excluded due to withdrawal of consent (Fig. 1). All participants underwent brain MRI including DCE MRI.

# Clinical evaluation

Baseline demographic and clinical characteristics of the participants were assessed, including diabetes, hypertension, dyslipidemia, cardiovascular disease history, and stroke history. Global cognitive assessment (MMSE and MoCA) was also conducted. These clinical data were collected within 1–2 months of the MRI examination.

# MRI protocol

All examinations were conducted using a 3 T scanner (MAGNETOM VIDA, Siemens Healthcare, Erlangen, Germany). Image sequences included sagittal 3D magnetization-prepared rapid acquisition with gradient echo imaging, axial T2-weighted imaging, axial susceptibility-weighted imaging, sagittal 3D T2-weighted FLAIR, coronal DCE MRI, and sagittal contrast-enhanced 3D T1-weighted black blood imaging (3D T1 BB),

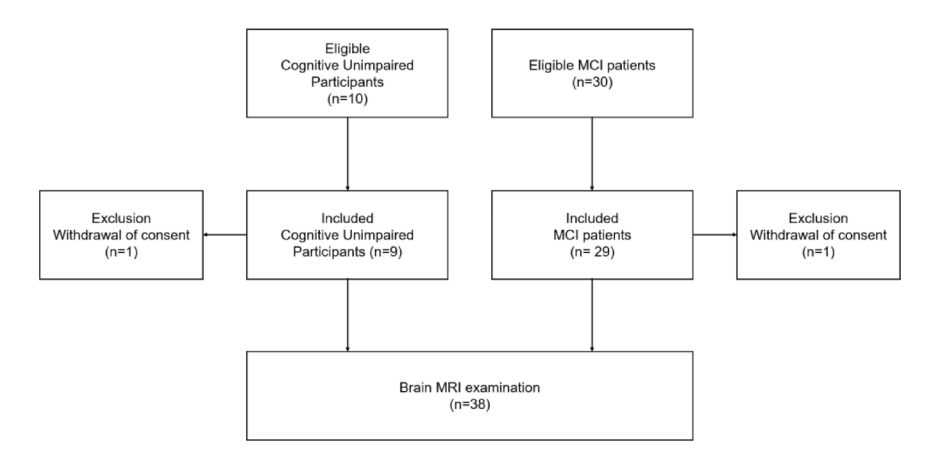


Fig. 1. Flowchart of patient inclusion.

chronologically. The parameters of each sequence are detailed in Supplementary Table 1. The DCE MRI was acquired using the golden-angle radial sparse parallel-volumetric interpolated breath-hold (GRASP-VIBE) sequence, and consisted of 92 series with time intervals of 6.2 s. Each series was composed of 30 sections of coronal images with 3.0-mm thickness, and acquired in an anterior-posterior direction with the level of the corpus callosum genu being the foremost plane. The following imaging parameters were used for the DCE MRI: repetition time, 6.24 ms; echo time, 2.91 ms; field of view, 240×240 mm; voxel size, 0.625×0.625×0.025×0.0 mm³. At the 10th dynamic phase, a gadolinium-based contrast agent was injected (0.1 mmol/kg; ProHance, Bracco, Milan, Italy) by an injector at a rate of 4 mL/s, followed by 30 mL of saline bolus. The total acquisition time for the DCE MRI was 9 min 32 s. After DCE MRI acquisition, contrast-enhanced 3D T1 BB imaging was acquired without additional contrast injection.

# Volumetric analysis using structural MRI

PSD was segmented by a region of interest (ROI) drawn section-by-section on contrast-enhanced 3D T1 BB images, using threshold-based algorithms implemented in ITK-SNAP (version 3.8.0) (Fig. 2). We identified the PSD as the enhancing structure located at the superior and lateral aspect of superior sagittal sinus (SSS), where meningeal lymphatic vessels predominantly locate, on contrast-enhanced 3D T1 BB images<sup>13,22,23</sup>. The operator applied a two-sided threshold to broadly define the ROI of PSD by generating a speed image, which assigns positive speed values to voxels likely representing the PSD and negative values to the background. Seed points were then placed within the ROI to initiate segmentation, and the contour evolved in real time, stopping when no further propagation was visible or when the contour leaked outside the boundaries<sup>24,25</sup>. The ROI delineation and manual editing was performed by a research assistant with 3 years of experience under supervision of a neuroradiologist (M.P.) with 9 years of experience, both of whom were blinded to all corresponding clinical information.

3D magnetization-prepared rapid acquisition with gradient echo images were uploaded to the volBrain online brain volumetry platform (https://www.volbrain.net/).<sup>26</sup> The volBrain pipeline automatically processes T1-weighted images through several steps, including denoising with an adaptive non-local mean filter, affine registration to the Montreal Neurological Institute (MNI) space using Advanced Normalization Tools (ANTs), N4 bias field correction to address image inhomogeneities, and intensity normalization<sup>27</sup>. Brain parenchyma segmentation is performed using a multi-atlas framework that combines nonlinear registration and patch-based label fusion<sup>28</sup>.

We analyzed total intracranial volume (ICV), cortical gray matter, and hippocampal volumes (measured in mL). To account for individual differences in head size, volumes of PSD, cortical gray matter, and hippocampus were adjusted for ICV in subsequent analyses.

# Functional analysis using DCE MRI

DCE MRI data were processed using a commercial software (nordicICE version 4.1.3; NordicNeuroLab, Bergen, Norway) to generate time-intensity curves for each ROI. To investigate the peak wash-in rate, wash-out rate, and time to peak enhancement of the PSD, circular ROIs were manually placed by a neuroradiologist (M.P.)

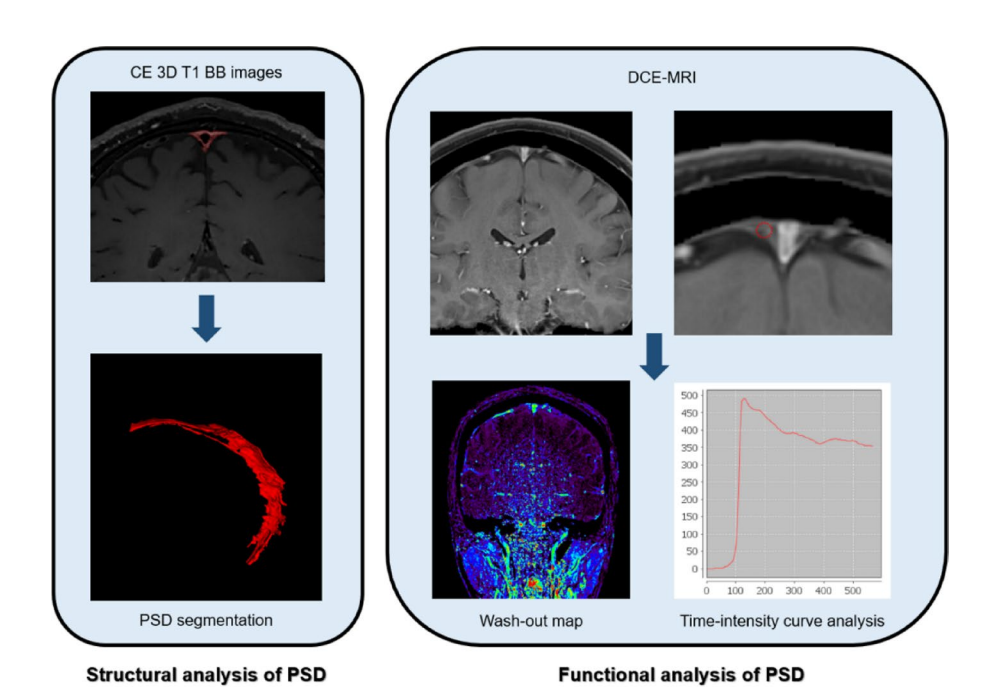


**Fig. 2.** Structural and functional imaging analysis of parasagittal dural space using brain MRI. DCE-MRI: dynamic contrast enhanced magnetic resonance imaging; CE 3D T1 BB images: contrast-enhanced 3-dimensional T1-weighted black-blood images.

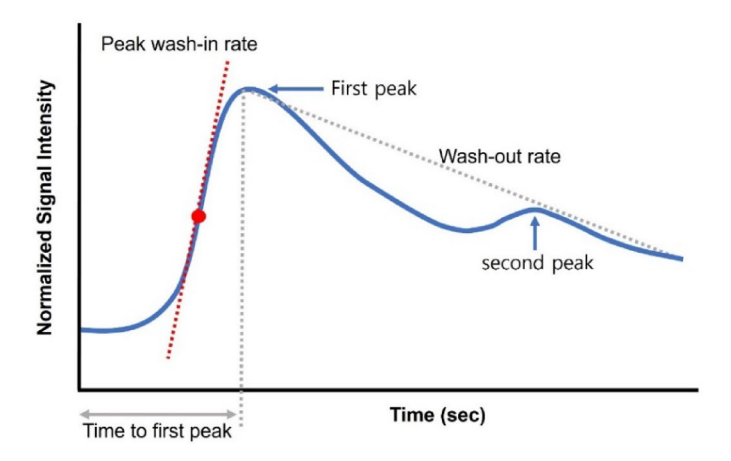


**Fig. 3.** A schematic presentation of time-intensity curve used as the basis for the assessment of DCE parameters of PSD. In cases where multiple signal peaks were observed, the first peak—defined as the phase when the signal reaches its initial peak and begins to decline, or reaches its first plateau—was used to calculate the time to the first peak.

with nine years of experience in neuroradiology, using contrast-enhanced 3D T1 BB and 3D T2 FLAIR images as references. The ROI on the PSD was placed in the superolateral aspect of the superior sagittal sinus (SSS), a region known to contain meningeal lymphatic vessels 13,22,23. Specifically, ROIs were located within the PSD adjacent to the SSS at the level of the parietal lobe, approximately within 1 cm anterior or posterior to the central sulcus, depending on individual anatomical variation. The mean ROI value from each dynamic phase of DCE MRI was then used to construct the signal-intensity curve. However, since signal intensity in MRI is not an absolute measure, direct estimation and analysis of DCE parameters using raw signal intensity may be problematic. To address this, the signal intensity was normalized as a percentage of its maximum value observed during the DCE MRI acquisition. This normalized intensity was then used to estimate the peak wash-in rate, wash-out rate, and time to first peak. Since some patients exhibited multiple enhancement peaks on the timeintensity curves, we utilized the time to the first peak enhancement, which was defined as the phase when the signal reaches its initial peak and begins to decline, or when it reaches its first plateau. The peak wash-in rate was defined as the maximum slope observed during the interval between the initiation of contrast agent injection (the 10th dynamic phase) and the occurrence of the first peak enhancement. Finally, the wash-out rate was defined as the slope between the first peak enhancement and the final acquisition time(Fig. 3). When the normalized signal intensity at the final acquisition time was the same as or higher than the value at the first peak enhancement, the wash-out rate was recorded as 0 to reflect the absence of wash-out for intra-observer reproducibility analysis, ROI placement was repeated by the same observer after four months. For inter-observer reproducibility, a second neuroradiologist (B.J., with six years of experience) independently performed ROI placement.

# Statistical analysis

Categorical data are shown as the number of observations (percentage), and continuous data are shown as the mean (standard deviation) or median (interquartile range [IQR]), according to the normality tests using Kolmogorov-Smirnov test. Demographic, clinical characteristics, and both morphologic and functional imaging-derived parameters were compared between the cognitively unimpaired elderly participants and MCI patients using the Mann–Whitney U test or Fisher's exact test.

To explore the relationship between cognitive function and the volume and functional parameters of PSD, while adjusting for other clinical and MRI-derived factors, univariate and multivariate linear regression analyses were sequentially performed twice—once with MMSE and once with MoCA scores as the dependent variables. The independent variables included age, sex, cortical gray matter volume, hippocampal volume, PSD volume, PSD peak wash-in rate, PSD wash-out rate, and time to first peak enhancement of PSD. Variables with a P-value of less than 0.1 in the univariate analysis were included as covariates in the multivariate regression analysis. For intra-observer reproducibility analysis, the estimated peak wash-in rate, wash-out rate, and time to first peak from ROI placement, repeated by the same observer after a four-month interval, were analyzed using intraclass correlation coefficient (ICC) analysis. For inter-observer reproducibility, the estimated peak wash-in rate, washout rate, and time to first peak from ROI placements by the first observer and a second neuroradiologist were assessed using the ICC method. In addition, the root mean square coefficient of variation (RMS-CoV) of signal intensity over time was calculated within each ROI to quantify intra-ROI signal variability across all subjects. This measure was used to complement the reproducibility assessment by providing a summary of temporal signal consistency within small ROI. Statistical analyses were performed using SPSS (version 25.0; IBM Corporation) and MedCalc (version 9.3.6.0; MedCalc Software). Statistical significance was accepted at a level of 0.05 (twotailed).

Variables	Cognitively Unimpaired (n=9)	MCI (n=29)	P value
Age (y)	74.0 (70-74.5)	76.0 (69-79.5)	0.196
Sex (M: F)	3:6	13:16	0.706
Hypertension	3 (33.3%)	14 (48.3%)	0.476
Diabetes mellitus	2 (22.2%)	7 (24.1%)	1.000
Dyslipidemia	1 (11.1%)	7 (24.1%)	0.650
MMSE	28.0 (25.0-28.5)	26.0 (24.0-27.0)	0.086
MoCA	26.0 (23.0-27.0)	23.0 (21.0-24.5)	0.021
ICV volume (mL)	1280.7 (1216.0-1440.5)	1335.1 (1250.5–1412.0)	0.595
Cortex (ratio of ICV)	0.45 (0.45-0.48)	0.46 (0.44-0.47)	0.482
Hippocampus (ratio of ICV x 10 <sup>3</sup> )	5.7 (5.6-6.3)	5.5 (4.6-6.1)	0.144

**Table 1**. Clinical and demographic characteristics of cognitively unimpaired participants and patients with MCI. MCI = Mild cognitive impairment, MMSE = Mini-Mental State Examination, MoCA = Montreal cognitive assessment. Data are medians with interquartile ranges in parentheses.

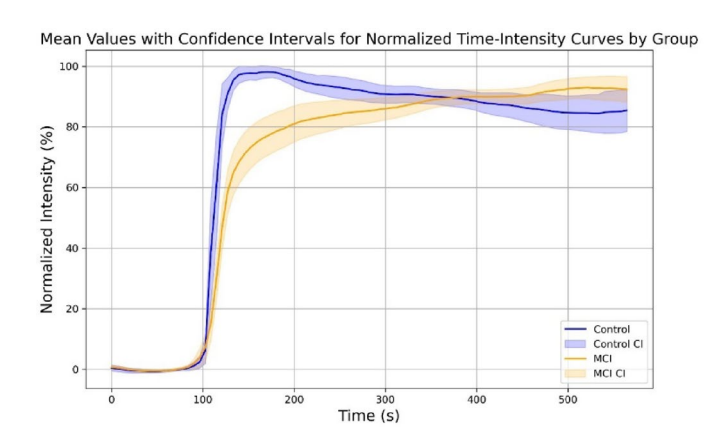


**Fig. 4.** Normalized time-intensity curves for PSD depicted with mean values and 95% confidence interval in cognitively unimpaired and MCI subjects.

### Results

# Clinical and demographic characteristics

This study included nine cognitively unimpaired elderly participants (median age, 74.0 years; interquartile range, 70–74.5 years; M:F = 3:6) and 29 patients with MCI (median age, 76.0 years; interquartile range, 69–79.5 years; M:F = 13:16). There were no differences in sex (P=0.196), age (P=0.706), the presence of hypertension (P=0.476), diabetes mellitus (P=1.000), or dyslipidemia (P=0.650) between the two groups (Table 1).

Patients with MCI had lower MMSE scores but it was not statistically significant compared with cognitively unimpaired participants (median, 26.0; interquartile range, 24.0–27.0 vs. median 28.0; interquartile range, 25.0-28.5, P=0.086). Patients with MCI had significantly lower MoCA score than cognitively unimpaired elderly participants (median, 23.0; interquartile range, 21.0-24.5 vs. median, 26.0; interquartile range, 23.0-27.0, P=0.021).

ICV, cortical gray matter (ratio of ICV  $\times$  10<sup>3</sup>), and hippocampus volumes (ratio of ICV  $\times$  10<sup>3</sup>) did not differ between cognitively unimpaired participants and MCI patients.

# Comparisons of the volume and DCE MRI parameters of PSD between cognitively unimpaired participants and MCI patients

PSD volume (ratio of ICV x  $10^3$ ) was significantly higher in MCI patients than in cognitively unimpaired participants (7.87 [interquartile range, 5.57–8.56] vs. 9.08 [interquartile range, 7.65–9.54], P = 0.023).

The median size of the placed ROI was  $5.078 \text{ mm}^2$  (interquartile range: 4.688-9.375). Peak wash-in rate was decreased in MCI patients (3.02 [interquartile range, 2.38-3.83]) than in cognitively unimpaired participants (5.23 [interquartile range, 4.25-5.96], P < 0.001) (Fig. 4). Time to first peak was prolonged in the MCI patients compared to the cognitively unimpaired participants (32.0 [interquartile range, 26.5-60.0] vs. 23.0 [interquartile range, 21.5-26.0], P = 0.001). On the other hand, wash-out rate of PSD was not significantly different between cognitively unimpaired participants and MCI patients (0.16 [interquartile range, 0.09-0.20] vs. 0.09 [interquartile range, 0.026-0.090], P = 0.390) (Table 2).

Variables	Cognitively Unimpaired (n=9)	MCI (n = 29)	P value
PSD volume (ratio of ICV x 10 <sup>3</sup> )	7.87 (5.57–8.56)	9.08 (7.65-9.54)	0.023
Peak wash-in rate (%/sec)	5.23 (4.25-5.96)	3.02 (2.38-3.83)	< 0.001
Wash-out rate (%/sec)	0.16 (0.09-0.20)	0.09 (0.026-0.090)	0.390
Time to first peak	23.0 (21.5–26.0)	32.0 (26.5-60.0)	0.001

**Table 2**. Comparisons of imaging parameters of PSD between cognitively unimpaired participants and patients with MCI. Data are medians with interquartile ranges in parentheses. PSD = parasagittal dural space, MCI = Mild cognitive impairment, ICV = intracranial volume.

n=38	Univariate			Multivariate		
Variables	Coefficient (β)	Standardized coefficient	P value	Coefficient (β)	Standardized coefficient	P value
Age (y)	- 0.079 (- 0.189-0.031)	- 0.236	0.154	-		-
Female sex	- 0.824 (- 2.424-0.776)	- 0.171	0.303	-		-
ICV volume (mL)	0.004 (- 0.001-0.010)	0.246	0.136	-		-
Cortex volume (ratio of ICV)	13.245 (- 22.632-49.121)	0.124	0.459			
Hippocampus volume (ratio of ICV x 10 <sup>3</sup> )	1.182 (0.207-2.157)	0.379	0.019	0.867 (-0.058-1.791)	0.278	0.065
PSD (ratio of ICV x 10 <sup>3</sup> )	- 0.550 (- 1.0740.025)	- 0.334	0.040	- 0.579 (- 1.072 0.086)	-0.352	0.023
Peak wash-in rate (%/sec)	0.404 (- 0.207-1.014)	0.218	0.188	-	-	-
Wash-out rate (%/sec)	- 2.984 (- 6.298-0.331)	- 0.291	0.076	- 3.293 (- 6.351 0.235)	- 0.321	0.036
Time to first peak	- 0.016 (- 0.062-0.030)	- 0.118	0.482	-	-	-

**Table 3.** Multivariable linear regression analysis for the association of MMSE score with the clinical and MRI-derived factors. MMSE = Mini-Mental State Examination, PSD = parasagittal dural space, ICV = intracranial volume.

# Association of the global cognitive score with volume and functional parameters of PSD

In the univariate linear analysis for MMSE score, hippocampus volume ( $\beta$ =1.182, 95% CI [0.207–2.157], P=0.019), PSD volume ( $\beta$ = -0.550, 95% CI [-1.074–-0.025], P=0.040), and wash-out rate ( $\beta$ = -2.984, 95% CI [-6.298–0.331], P=0.076) showed significant associations with the MMSE score, with p value of less than 0.1. Other variables, including age ( $\beta$ = -0.079, 95% CI [-0.189–0.031], P=0.154), female sex ( $\beta$ = -0.824, 95% CI [-2.424–0.776], P=0.303), ICV volume ( $\beta$ =0.004, 95% CI [-0.001–0.010], P=0.136), cortex volume ( $\beta$ =13.245, 95% CI [-2.2632–49.121], P=0.459), peak wash-in rate ( $\beta$ =0.404, 95% CI [-0.207–1.014], P=0.188), and time to first peak ( $\beta$ = -0.016, 95% CI [-0.062–0.030], P=0.482), were not significantly associated with the MMSE score. In the multivariate analysis, PSD volume ( $\beta$ =-0.579, 95% CI [-1.072–-0.086], P=0.023) and wash-out rate ( $\beta$ =-3.293, 95% CI [-6.351–-0.235], P=0.036) remained significantly associated with the MMSE score (Table 3).

In the univariate linear analysis for MoCA score, the cortical gray matter volume ( $\beta$  = 30.171, 95% CI [-5.860–66.202], P = 0.098), peak wash-in rate ( $\beta$  = 0.665, 95% CI [0.057–1.272], P = 0.033) and the hippocampus ratio ( $\beta$  = 1.226, 95% CI [0.216–2.236], P = 0.019) were associated with the MoCA score, showing p value of less than 0.1. The volume of PSD volume ( $\beta$  = -0.367, 95% CI [-0.930–0.196], P = 0.195), wash-out rate ( $\beta$  = -1.822, 95% CI [-5.357–1.713], P = 0.303) or time to first peak ( $\beta$  = -0.003, 95% CI [-0.050–0.045], P = 0.909) of PSD was not significantly associated with MoCA score (Table 4).

In the multivariate analysis with the three co-variables, the peak wash-in rate remains significant ( $\beta$  = 0.614, 95% CI [0.019–1.209], P = 0.043), after adjustment of cortical gray matter volume and hippocampal volume.

The associations between MoCA subdomain scores and PSD volume and functional parameters are presented in the supplementary material (Supplementary Tables 2-7).

# Intra-observer and inter-observer reproducibility analysis for DCE MRI parameters

The intra-observer ICC for wash-in rate, wash-out rate, and time to first peak were 0.924 (95% CI: 0.860–0.960), 0.685 (95% CI: 0.471–0.823), and 0.776 (95% CI: 0.610–0.877), respectively. The inter-observer ICC for wash-in rate, wash-out rate, and time to first peak were 0.843 (95% CI: 0.716–0.916), 0.856 (95% CI: 0.738–0.923), and 0.925 (95% CI: 0.859–0.961), respectively. The RMS-CoV for ROI measurements of the PSD was 38.4%, ranging from 14.8 to 68.3%.

## Discussion

The results of the study show a significant morphologic and functional differences in imaging parameters of PSD between cognitively unimpaired elderly participants and patients with MCI, indicating that MCI patients have a higher PSD volume, a lower peak wash-in rate, and a delayed time to peak. Additionally, a significant association was found between the PSD volume, wash-out rate, or peak wash-in rate with global cognitive function, suggesting that a functional changes of PSD may be associated with poor overall cognitive function.

n=38	Univariate			Multivariate		
Variables	Coefficient (β)	Standardized Coefficient	P value	Coefficient (β)	Standardized Coefficient	P value
Age (y)	- 0.060 (- 0.176-0.055)	-0.174	0.297	-		-
Female sex	- 0.517 (- 2.190-1.156)	-0.104	0.535	-		-
ICV volume (mL)	0.002 (- 0.004-0.008)	0.096	0.565	-		-
Cortex volume (ratio of ICV)	30.171 (- 5.860-66.202)	0.272	0.098	18.378 (-21.482-58.237)	0.166	0.355
Hippocampus volume (ratio of ICV x 10 <sup>3</sup> )	1.226 (0.216-2.236)	0.380	0.019	0.788 (-0.385-1.961)	0.244	0.181
PSD (ratio of ICV x 10 <sup>3</sup> )	- 0.367 (- 0.930-0.196)	-0.215	0.195	-		-
Peak wash-in rate (%/sec)	0.665 (0.057-1.272)	0.347	0.033	0.614 (0.019-1.209)	0.320	0.043
Wash-out rate (%/sec)	- 1.822 (- 5.357-1.713)	-0.172	0.303	-		-
Time to first peak	- 0.003 (- 0.050-0.045)	-0.019	0.909	-		-

**Table 4**. Multivariable linear regression analysis for the association of MoCA score with the clinical and MRI-derived factors. MoCA = Montreal cognitive assessment, PSD = parasagittal dural space, ICV = intracranial volume.

Several previous imaging studies have revealed morphological changes of PSD in humans with aging, showing the association between an increase in PSD volume or thickness and aging  $^{14-16}$ . This finding has been thought to reflect the age-related meningeal lymphatic dysfunction  $^{14}$ . However, those results were derived solely from subjects who were cognitively unimpaired. A previous study on Alzheimer's disease showed a positive correlation between PSD volume and global A $\beta$  burden, assessed via PET-CT scan<sup>29</sup>. However, the study included a small number of patients and lacked a comparison with controls. Therefore, there has been no previous study that directly compared the effect of normal aging and MCI, an early stage in the Alzheimer's disease spectrum, on PSD morphology. In this regard, we included both cognitively unimpaired elderly participants and patients with MCI, and observed that the volume of the PSD was greater in MCI patients compared to that of cognitively unimpaired subjects. Further, we observed that independent negative association between PSD volume and MMSE. This result seems to be in line with those previous reports, considering the association of meningeal lymphatic dysfunction with aging and neurodegeneration  $^{5,12,17}$ . Since accelerated brain aging is the major mechanism of cognitive decline in both MCI and AD, increased PSD volume in MCI patients may be understood as an imaging finding of accelerated aging occurring in the Alzheimer's and related diseases  $^{30-32}$ .

In addition to the morphologic aspect of the PSD, several previous studies have focused on its functional aspect of PSD using dynamic MRI following intravenous administration of a contrast agent 17-19,33. Despite differences in the detailed methods and metrics across the studies, a common suggested finding is the that impaired uptake or drainage of contrast agents in the meningeal lymphatic vessels is associated with aging, Parkinson's disease, and cerebral small vessel disease<sup>17,19,33</sup>. This study found that patients with MCI exhibit slower wash-in and delayed time to peak compared to cognitively unimpaired participants, suggesting that MCI subjects require more time for gadolinium contrast agents to migrate from vessels to the meningeal lymphatic system. These findings align with previous observations of impaired meningeal lymphatic uptake in Parkinson's disease using DCE MRI<sup>17</sup>. They also showed prolonged time to peak and decreased wash-in rate of PSD in Parkinson's disease group compared to normal controls or even multiple system atrophy or progressive supranuclear palsy subjects. According to previous animal studies, decreased meningeal lymphatic drainage led to exacerbated deposition of A $\beta$  in the meninges and the brain<sup>5,6</sup>. This outcome is thought to result from impaired A $\beta$  glymphatic efflux due to reduced meningeal lymphatic function, preventing proper drainage of  $A\beta$  from the CSF into the deep cervical lymph nodes<sup>5,6</sup>. Furthermore, exploratory multivariable linear regression analyses revealed a significant association between delayed wash-in rate or wash-out rate and global cognitive function, suggesting that delayed glymphatic efflux may be related to the disease severity in MCI patients. Given that amyloid or tau accumulation, a consequence of meningeal lymphatic dysfunction, occurs even before symptoms develop<sup>34</sup>, our results suggest the potential of DCE MRI as an early imaging marker for assessing disease severity in MCI or AD.

In addition, our findings suggest that both structural MRI and DCE MRI may reveal dysfunction of meningeal lymphatic system. Moreover, the enlarged PSD volume indicates potential dysfunction of meningeal lymphatic system, likely due to lymphatic stasis. Further studies are warranted to clarify the role and limitations of both structural and DCE MRI in the in vivo evaluation of the meningeal lymphatic system, employing a larger sample and various neurological conditions.

In previous dynamic MRI studies that evaluated the meningeal lymphatic system with intravenous administration of a contrast agent, some employed DCE MRI with a scan time of fewer than 10 min<sup>17,19</sup>, similar to this study, while others utilized multiple time points MRI spanning several hours<sup>18,33</sup>. Interestingly, the time of peak enhancement in the PSD following contrast agent administration was much shorter in the DCE MRI studies, taking less than 10 min, compared to the multiple-time-point MRI studies, which showed a range of around 20 min to 1 h. This difference may be due to the various features of the gadolinium-based contrast agent used, such as molecular size, lipophilicity, and charge, potentially resulting in a different kinetics<sup>18</sup>. Furthermore, in DCE MRI studies with shorter scan times, it is believed that the contrast agent in the PSD moves directly from the meningeal blood vessels, which are fenestrated and lack blood-meningeal barriers, resulting in faster peak enhancement<sup>17,35</sup>. This explanation is further supported by a recent study where fluorescent tracers (3 kDa dextran) injected intravenously rapidly leaked out from the vessels and accumulated in perivascular macrophages of the dural area<sup>36</sup>. This suggests that dural vessels possess more permeable endothelium without

a blood-brain barrier, allowing even large molecular weight substances, like 3 kDa dextran, to pass through. Considering that, a gadolinium-based contrast agent has a molecular weight of only about 0.6 kDa, its rapid movement and accumulation are consistent with this mechanism<sup>37</sup>. Conversely, in studies employing a longer time span with relatively longer scan-to-scan intervals, the delayed peak enhancement of the PSD may partially originate from the glymphatic system, reflecting the movement of the contrast agent as it passes through the blood-brain barrier, brain ICF and CSF, and eventually reaches the meningeal lymphatic vessels. Additional research is warranted to further elucidate this issue.

There are some limitations in our study. First, our study is a cross-sectional study with a small sample size, and thus, our observations need careful interpretations. Future studies should focus on the longitudinal changes in PSD volume and dynamics and their interactions with cognitive dysfunction. Second, we did not assess the amyloid and tau accumulation status of the participants, which might have close relationship with meningeal lymphatic activity. Third, although we used a contrast media injector to minimize variability in the contrast injection, individual differences in cardiac output may have influenced the time-intensity curve, particularly the time to the first peak. Furthermore, the small number of voxels included in each ROI may have contributed to some degree of signal variability, as reflected by moderately elevated RMS-CoV values. While this does not invalidate the findings, it should be considered when interpreting the ROI-based measurements.

In conclusion, this study demonstrates significant morphologic and functional differences in the PSD between cognitively unimpaired elderly individuals and patients with MCI. The findings suggest that differences in PSD volume and contrast agent dynamics between MCI and cognitively unimpaired subjects may reflect alterations in meningeal lymphatic function, which could be associated with early changes related to cognitive decline. Further research with larger cohorts is needed to validate these results and explore the potential of DCE MRI for early detection of neurodegenerative diseases.

# Data availability

The datasets generated during and/or analyzed during the current study are available from the corresponding author on reasonable request.

Received: 12 November 2024; Accepted: 18 June 2025

Published online: 04 July 2025

# References

- 1. Aspelund, A. et al. A dural lymphatic vascular system that drains brain interstitial fluid and macromolecules. *J. Exp. Med.* 212, 991–999. https://doi.org/10.1084/jem.20142290 (2015).
- Louveau, A. et al. Structural and functional features of central nervous system lymphatic vessels. Nature 523, 337–341. https://doi.org/10.1038/nature14432 (2015).
- 3. de Alves, K., Rustenhoven, J. & Kipnis, J. Meningeal immunity and its function in maintenance of the central nervous system in health and disease. *Annu. Rev. Immunol.* 38, 597–620. https://doi.org/10.1146/annurev-immunol-102319-103410 (2020).
- Da Mesquita, S., Fu, Z. & Kipnis, J. The meningeal lymphatic system: A new player in neurophysiology. Neuron 100, 375–388. https://doi.org/10.1016/j.neuron.2018.09.022 (2018).
- Da Mesquita, S. et al. Functional aspects of meningeal lymphatics in ageing and alzheimer's disease. Nature 560, 185–191. https://doi.org/10.1038/s41586-018-0368-8 (2018).
- Da Mesquita, S. et al. Meningeal lymphatics affect microglia responses and anti-Abeta immunotherapy. Nature 593, 255–260. https://doi.org/10.1038/s41586-021-03489-0 (2021).
- 7. Park, M., Park, J. P., Kim, S. H. & Cha, Y. J. Evaluation of dural channels in the human parasagittal dural space and dura mater. *Ann. Anat.* 244, 151974. https://doi.org/10.1016/j.aanat.2022.151974 (2022).
- 8. Zou, W. et al. Blocking meningeal lymphatic drainage aggravates parkinson's disease-like pathology in mice overexpressing mutated alpha-synuclein. *Transl. Neurodegener.* 8, 7. https://doi.org/10.1186/s40035-019-0147-y (2019).
- 9. Ringstad, G. & Eide, P. K. Cerebrospinal fluid tracer efflux to parasagittal dura in humans. Nat. Commun. 11 https://doi.org/10.10 38/s41467-019-14195-x (2020).
- 10. Rustenhoven, J. et al. Functional characterization of the dural sinuses as a neuroimmune interface. *Cell* **184**, 1000–1016e1027. https://doi.org/10.1016/j.cell.2020.12.040 (2021).
- 11. Shah, T. et al. Arachnoid granulations are lymphatic conduits that communicate with bone marrow and dura-arachnoid stroma. *J. Exp. Med.* 220 https://doi.org/10.1084/jem.20220618 (2023).
- 12. Zhou, Y. et al. Impairment of the glymphatic pathway and putative meningeal lymphatic vessels in the aging human. *Ann. Neurol.* 87, 357–369. https://doi.org/10.1002/ana.25670 (2020).
- 13. Absinta, M. et al. Human and nonhuman primate meninges harbor lymphatic vessels that can be visualized noninvasively by MRI. *Elife* 6 https://doi.org/10.7554/eLife.29738 (2017).
- Albayram, M. S. et al. Non-invasive MR imaging of human brain lymphatic networks with connections to cervical lymph nodes. Nat. Commun. 13, 203. https://doi.org/10.1038/s41467-021-27887-0 (2022).
- 15. Hett, K. et al. Parasagittal dural space and cerebrospinal fluid (CSF) flow across the lifespan in healthy adults. *Fluids Barriers CNS*. 19, 24. https://doi.org/10.1186/s12987-022-00320-4 (2022).
- Park, M., Kim, J. W., Ahn, S. J., Cha, Y. J. & Suh, S. H. Aging is positively associated with Peri-Sinus lymphatic space volume: assessment using 3T Black-Blood MRI. J. Clin. Med. 9 https://doi.org/10.3390/jcm9103353 (2020).
- 17. Ding, X. B. et al. Impaired meningeal lymphatic drainage in patients with idiopathic parkinson's disease. *Nat. Med.* 27, 411–418. https://doi.org/10.1038/s41591-020-01198-1 (2021).
- 19. Joo, B., Park, M., Ahn, S. J. & Suh, S. H. Assessment of meningeal lymphatics in the parasagittal dural space: A prospective feasibility study using dynamic Contrast-Enhanced magnetic resonance imaging. *Korean J. Radiol.* https://doi.org/10.3348/kjr.202 2.0980 (2023).
- Petersen, R. C. et al. Mild cognitive impairment: clinical characterization and outcome. Arch. Neurol. 56, 303–308. https://doi.org/10.1001/archneur.56.3.303 (1999).
- 21. Nasreddine, Z. S. et al. The Montreal cognitive assessment, moca: a brief screening tool for mild cognitive impairment. *J. Am. Geriatr. Soc.* 53, 695–699. https://doi.org/10.1111/j.1532-5415.2005.53221.x (2005).

- 22. Goodman, J. R., Adham, Z. O., Woltjer, R. L., Lund, A. W. & Iliff, J. J. Characterization of dural sinus-associated lymphatic vasculature in human alzheimer's dementia subjects. *Brain Behav. Immun.* 73, 34–40. https://doi.org/10.1016/j.bbi.2018.07.020 (2018).
- 23. Visanji, N. P., Lang, A. E. & Munoz, D. G. Lymphatic vasculature in human dural superior sagittal sinus: implications for neurodegenerative proteinopathies. *Neurosci. Lett.* 665, 18–21. https://doi.org/10.1016/j.neulet.2017.11.001 (2018).
- 24. Yushkevich, P. A. et al. User-Guided segmentation of Multi-modality medical imaging datasets with ITK-SNAP. *Neuroinformatics* 17, 83–102. https://doi.org/10.1007/s12021-018-9385-x (2019).
- 25. Gau, K. et al. Accuracy and practical aspects of semi- and fully automatic segmentation methods for resected brain areas. *Neuroradiology* 62, 1637–1648. https://doi.org/10.1007/s00234-020-02481-1 (2020).
- Manjon, J. V., Coupe, P. & volBrain An online MRI brain volumetry system. Front. Neuroinform. 10, 30. https://doi.org/10.3389/fn inf.2016.00030 (2016).
- 27. Nyul, L. G. & Udupa, J. K. On standardizing the MR image intensity scale. Magn. Reson. Med. 42, 1072-1081. (1999).
- 28. Coupe, P., Manjon, J. V., Chamberland, M., Descoteaux, M. & Hiba, B. Collaborative patch-based super-resolution for diffusion-weighted images. *Neuroimage* 83, 245–261. https://doi.org/10.1016/j.neuroimage.2013.06.030 (2013).
- 29. Song, A. K. et al. Parasagittal dural space hypertrophy and amyloid-beta deposition in alzheimer's disease. *Brain Commun.*. https://doi.org/10.1093/braincomms/fcad128 (2023).
- 30. Beheshtt, I., Maikusa, N. & Matsuda, H. The association between Brain-Age score (BAS) and traditional neuropsychological screening tools in alzheimer's disease. *Brain Behav.* 8, e01020. https://doi.org/10.1002/brb3.1020 (2018).
- 31. Elliott, M. L. MRI-based biomarkers of accelerated aging and dementia risk in midlife: how close are we? Ageing Res. Rev. 61, 101075. https://doi.org/10.1016/j.arr.2020.101075 (2020).
- 32. Huang, W. et al. Accelerated brain aging in amnestic mild cognitive impairment: relationships with individual cognitive decline, risk factors for alzheimer disease, and clinical progression. *Radiol. Artif. Intell.* 3, e200171. https://doi.org/10.1148/ryai.2021200171 (2021).
- 33. Zhang, M. et al. Evaluation of glymphatic-meningeal lymphatic system with intravenous gadolinium-based contrast-enhancement in cerebral small-vessel disease. *Eur. Radiol.* https://doi.org/10.1007/s00330-023-09796-6 (2023).
- 34. Jack, C. R. Jr. et al. Tracking pathophysiological processes in alzheimer's disease: an updated hypothetical model of dynamic biomarkers. *Lancet Neurol.* 12, 207–216. https://doi.org/10.1016/S1474-4422(12)70291-0 (2013).
- 35. Mezey, E. et al. An immunohistochemical study of lymphatic elements in the human brain. *Proc. Natl. Acad. Sci. U S A.* 118 https://doi.org/10.1073/pnas.2002574118 (2021).
- Merlini, A. et al. Distinct roles of the meningeal layers in CNS autoimmunity. Nat. Neurosci. 25, 887–899. https://doi.org/10.1038/s41593-022-01108-3 (2022).
- 37. Caravan, P., Ellison, J. J., McMurry, T. J. & Lauffer, R. B. Gadolinium(III) chelates as MRI contrast agents: structure, dynamics, and applications. *Chem. Rev.* 99, 2293–2352. https://doi.org/10.1021/cr980440x (1999).

# **Acknowledgements**

none

# **Author contributions**

The authors confirm contribution to the paper as follows: study conception and design: M.P.; data collection: H.K.K., H.C., and C.H.L.; analysis and interpretation of results: B.J.; draft manuscript preparation: B.J. and M.P.; manuscript editing: S.S.K, S.S.A., A.S.J, and S.H.S. All authors reviewed the results and approved the final version of the manuscript.

### Funding

This work was supported by the National Research Foundation of Korea(NRF) grant funded by the Korea government(MSIT) (No. NRF-2020R1C1C1005724 and No. RS-2023-00270209) and by Bracco Diagnostics Inc.

# **Declarations**

# Competing interests

The authors declare no competing interests.

# Additional information

**Supplementary Information** The online version contains supplementary material available at https://doi.org/10.1038/s41598-025-07909-3.

**Correspondence** and requests for materials should be addressed to M.P.

Reprints and permissions information is available at www.nature.com/reprints.

**Publisher's note** Springer Nature remains neutral with regard to jurisdictional claims in published maps and institutional affiliations.

**Open Access** This article is licensed under a Creative Commons Attribution-NonCommercial-NoDerivatives 4.0 International License, which permits any non-commercial use, sharing, distribution and reproduction in any medium or format, as long as you give appropriate credit to the original author(s) and the source, provide a link to the Creative Commons licence, and indicate if you modified the licensed material. You do not have permission under this licence to share adapted material derived from this article or parts of it. The images or other third party material in this article are included in the article's Creative Commons licence, unless indicated otherwise in a credit line to the material. If material is not included in the article's Creative Commons licence and your intended use is not permitted by statutory regulation or exceeds the permitted use, you will need to obtain permission directly from the copyright holder. To view a copy of this licence, visit <a href="https://creativecommons.org/licenses/by-nc-nd/4.0/">https://creativecommons.org/licenses/by-nc-nd/4.0/</a>.

© The Author(s) 2025